

Article

# A Method to Fit Phase Diagrams of Slow-Rotation Pulsars with Accretion Columns

Rodrigo R. Silva <sup>1,†,‡</sup>, Rafael C. R. de Lima <sup>2,\*</sup>, Jaziel G. Coelho <sup>1,3,‡</sup>, Paulo E. Stecchini <sup>1,4,‡</sup>,  
Caroline M. de Liz <sup>2,‡</sup> and José C. N. de Araujo <sup>1,†,‡</sup>

<sup>1</sup> Divisão de Astrofísica, Instituto Nacional de Pesquisas Espaciais, Avenida dos Astronautas 1758, São José dos Campos 12227-010, SP, Brazil

<sup>2</sup> Departamento de Física, Universidade do Estado de Santa Catarina, Joinville 89219-710, SC, Brazil

<sup>3</sup> Núcleo de Astrofísica e Cosmologia (Cosmo-Ufes), Departamento de Física, Universidade Federal do Espírito Santo, Vitória 29075-910, ES, Brazil

<sup>4</sup> Instituto de Astronomia, Geofísica e Ciências Atmosféricas, Universidade de São Paulo, São Paulo 05508-900, SP, Brazil

\* Correspondence: rafael.lima@udesc.br

† These authors contributed equally to this work.

‡ These authors contributed equally to this work.

**Abstract:** We demonstrate a method to simulate a pulse profile of the emission of accretion columns in a neutron star. Given a set of parameters that characterize the star, e.g., mass and radius, and the positions and shapes of the accretion columns, the pulse profile can be calculated and compared with real data. Some characteristics of phase diagrams are shown considering an accretion column in the form of a cone trunk and also in the form of a cylinder. Furthermore, in our first approach we develop a combination between a genetic algorithm and a Bayesian sampling algorithm to constrain some variables. Finally, as an example, we apply the method to observed data of source 1A 0535+262.

**Keywords:** 1A 0535+262; accretion column; pulse profile



**Citation:** Silva, R.R.; de Lima, R.C.R.; Coelho, J.G.; Stecchini, P.E.; de Liz, C.M.; de Araujo, J.C.N. A Method to Fit Phase Diagrams of Slow-Rotation Pulsars with Accretion Columns. *Galaxies* **2023**, *11*, 18. <https://doi.org/10.3390/galaxies11010018>

Academic Editors: Roberto Mignani and Yosuke Mizuno

Received: 29 September 2022

Revised: 9 January 2023

Accepted: 12 January 2023

Published: 16 January 2023



**Copyright:** © 2023 by the authors. Licensee MDPI, Basel, Switzerland. This article is an open access article distributed under the terms and conditions of the Creative Commons Attribution (CC BY) license (<https://creativecommons.org/licenses/by/4.0/>).

## 1. Introduction

Pulsars are compact objects with emission characterized by the beam of radiation emitted from their magnetic poles. In binary systems, there can be an accretion of matter from the companion star to the magnetic poles of the pulsar, forming what are called accretion columns [1]. Accreting millisecond X-ray pulsars (AMXPs) are believed to be neutron stars in low mass X-ray binaries [2].

The accretion columns formed in those systems can have several shapes as filled funnel, hollow funnel, and pancaked or spaghetti (when instabilities are predominant) [1]. The filled funnel occurs when infalling matter comes with spherical symmetry [3]. The photons scattered through the walls of the column are called fan beam, whereas the photons that go upwards compound a pencil beam. Even though the type of emission is related to the accretion rate, a combination of fan beam and pencil beam cannot be discarded [4].

Falkner [5] developed a three-dimensional full cylindrical-shaped antipodal accretion column simulation and used the Beloborodov ray-tracing model [6] to calculate the pulse profile formed by the X-ray photons coming from the column. There, the geodesics were determined through the bilinear interpolation of some integrated points from the surface. The hot spots may have arbitrary sizes and locations (see also [7]). Furthermore, we allow different shapes for the accretion columns, e.g., cone trunk and cylindrical, as illustrated in Figure 1.

One pulsar believed to have accretion columns is 1A 0535+262, one of the best-studied high mass X-ray binary (HMXB) of the galaxy. The system is composed of a Be star and a neutron star with an orbital period of  $\sim 111$  d [8] and a spin period of  $\sim 104$  s [9]. From this pulsar, Doroshenko [10] has noted a spectral softening that could be explained by the

presence of accretion columns. Caballero [11] has done a pulse profile decomposition and found a good match with a neutron star  $M = 1.4 M_{\odot}$ ,  $R = 10$  km and an accretion column height of 0.5 km.

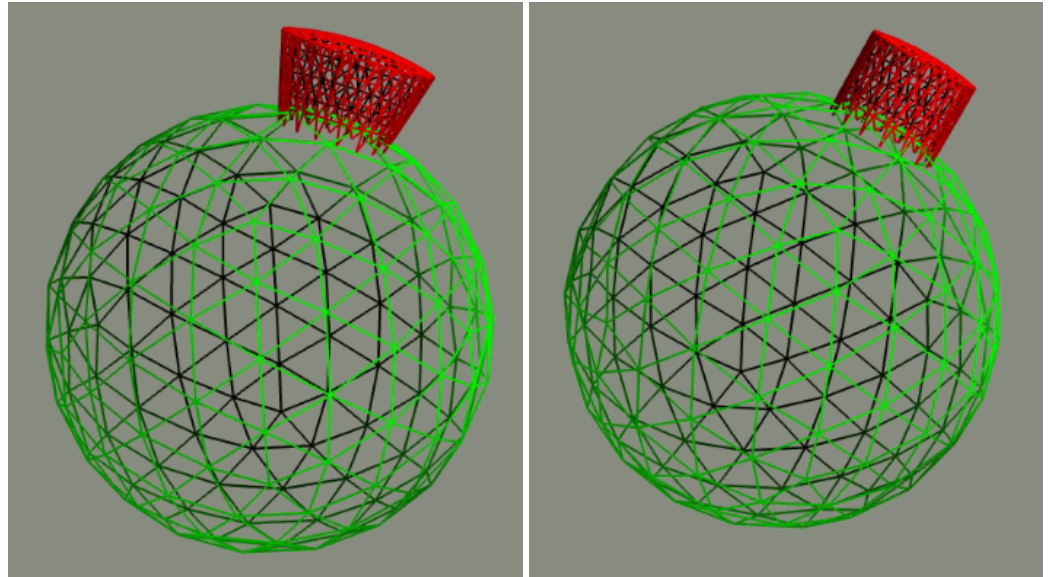


**Figure 1.** Two columns shapes, cone trunk shape in the left, and a cylindrical shape in the right.

1A 0535+262 long spin period makes it unnecessary to consider fast spin effects. The data available from the NuSTAR mission covers hundreds of spin periods and takes place in a quiescent phase of the source, making 1A 0535+262 a good candidate for finding accretion-column effects on its phase diagram.

The main goal of the present paper is to reproduce the emission profile in the X-ray range of these accretion columns, in a star with two columns in independent positions, taking into account a Schwarzschild spacetime, gravitational redshift, and the relativistic Doppler effect. The simulation creates a three-dimensional structure of the columns, with cylindrical or conical shapes with cap-like structures in the bottom and top of the columns. At the same time, we created a table from integration with the results of the photon geodesics. By the bilinear interpolation of the table data, we found the emission angle and the impact parameter for each column emission point. The resulting simulation was in agreement with other studies carried out, and we compared its aspects for different column heights, column shapes and positions, and star radii. We then used algorithms for sampling (the genetic algorithm and Markov Monte Carlo chain) to determine the best parameters that described the pulse profile of the source 1A 0535+262.

To do so, this paper is organized as follows. In Section 2, we present how the calculations are done and discuss the obtained results. Finally, in Section 3 we summarize the main conclusions and remarks about them.

## 2. Materials and Methods

In this section, we introduce the steps taken into our simulation of a neutron star with accretion columns. The parameters considered are the neutron star mass  $M$ , its radius  $R$ , the angular frequency  $f$ , and the angle of its rotational axis with the line of sight (LOS)  $i$ . We also have the parameters of the columns' positions and shape, which are the semi-aperture angle  $\theta_0$ ; its latitude  $\theta$ ; its longitude  $\phi$ , where the north was set to the column rotational axis; its column height  $H$ ; and its column temperature  $T$ . Some of those coordinates are illustrated in Figure 2.

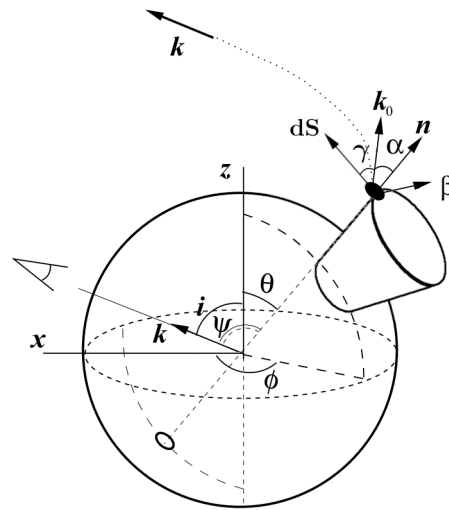


**Figure 2.** The coordinate system adopted for a photon leaving in the  $\vec{k}_0$  direction from a small region with area  $dS$  on the side of the cone trunk accretion column of the neutron star. The rotational axis is the z-axis,  $\vec{k}$  points towards the observer, and  $\vec{\beta}$  is the velocity.

The simulation was designed in python following the recipe described by Falkner [5]. Therefore, it was developed by following the steps below:

1. Lookuptable: For some values of possible positions where photons can leave the columns, we created a table with their point of emission and emission angle  $\alpha$ .
2. Object creation: From a given set of parameters of the columns  $(\theta_0, \theta, \phi, H)$ , a 3D mesh of the star was created, where the coordinates of the baricenter of its divisions can be taken and followed through the star's rotation and the columns can be shaped as we want.
3. Flux calculation: Given a set of parameters  $(M, R, f, i, \theta_0, \theta, \phi, H, T)$ , the flux that comes from each point of the column was calculated and summed for each phase of the star's rotation.

To calculate the geodesics, Schwarzschild spacetime was assumed and, to the flux, the effects of the Doppler shift and gravitational redshift were also considered. Following the above steps, we use the model to fit some data sets. For example, we apply the model to the source 1A 0535+262, discovered in 1975 by Ariel V [9], through sampling algorithms. In that step, Markov Chain Monte Carlo (MCMC) and the genetic algorithm (GA) were employed to constrain the values of the set  $(M, R, f, i, \theta_0, \theta, \phi, H, T)$ , which has the best fit with source 1A 0535+262.

### 2.1. Lookuptable

In the simulation, we want to calculate the flux emitted from a given point in the accretion column with polar coordinates  $R$  and  $\Psi$ , where  $\Psi$  is the angle between the position and the observer's line of sight. In order to do this, we need to obtain the angle of emission  $\alpha$ , which is the angle between the photon direction and the surface normal, and the impact parameter  $b$ . Those parameters can be obtained by solving the geodesics for the photons, for a Schwarzschild spacetime in our model. In our case, we need to be careful because in some cases the photons may approach the star before leaving it, i.e., there are trajectories with periastron. This scenario is a consequence of the photons leaving from a point above the surface of the star. The Figure 3 shows the two kinds of trajectories.

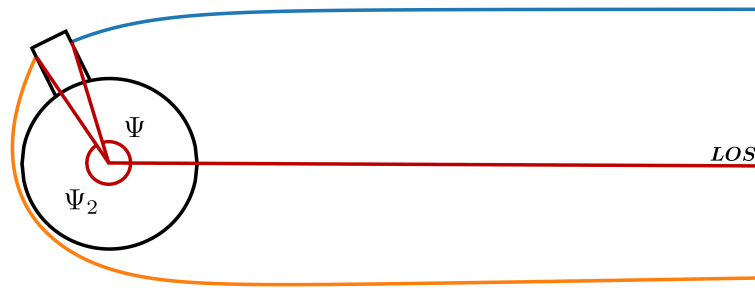


**Figure 3.** Two possible trajectories for the fan beam of an accretion column. The blue one shows a trajectory in which the periastron is the emitting point. The yellow trajectory has a periastron along the way, and the emitting point is positioned on the back of the column.

The solution needs to be taken apart in two steps, one where the photon goes from the emission point to the periastron and another where it leaves the periastron and goes to the observer. Therefore, one needs to know beforehand if the trajectory has a periastron or not. To do that,  $\Psi$  is calculated from a list of  $R$  and  $\alpha$  through numerical integration, i.e.,

$$\Psi(R) = \int_R^{\infty} \frac{1}{r^2} \left[ \frac{1}{b^2} - \left(1 - \frac{r_s}{r}\right) \frac{1}{r^2} \right]^{-1/2} dr, \quad (1)$$

where  $r_s = 2M$  is the Schwarzschild radius, where it is used the geometric unit system with  $G = c = 1$ . This is solved by Romberg's method provided by the SCIPY library for Python. The impact parameter is related to  $R$  and  $\alpha$  through the expression

$$\sin(\alpha) = \frac{b}{R} \sqrt{1 - \frac{r_s}{R}}. \quad (2)$$

When  $\alpha > \pi/2$ , the trajectory has a periastron and then the angle between its radial direction and the LOS,  $\Psi^*$ , is

$$\Psi^*(R) = 2\Psi(r_p) - \Psi(R), \quad (3)$$

where  $\Psi(r_p)$  is the same angle when the photon is precisely on the periastron and  $\Psi(R)$  is the angle when it crosses the emitting radius. Further, knowing that  $\alpha^* = \pi - \alpha$ ,  $\Psi(R)$  can be retrieved via bilinear interpolation from a table containing the values for  $R$ ,  $\Psi$ , and  $\alpha$ . Therefore, we are able to read from this table the value for any  $\alpha$ , given  $R$  and  $\Psi$  through bilinear interpolation; see Figure 4.

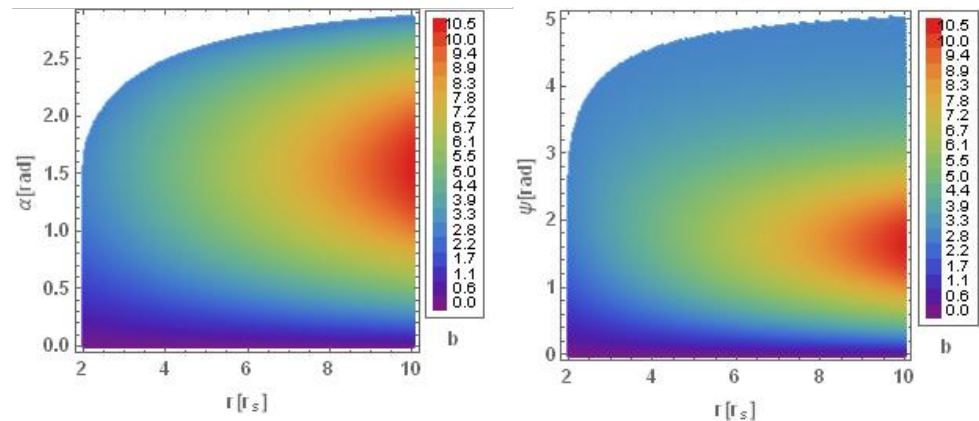


**Figure 4.** Relations between the parameters ( $R$ ,  $\Psi$ ,  $b$ ,  $\alpha$ ). The two figures shows the distribution in the  $r - \alpha$  and  $r - \Psi$  plane, respectively. The colors are associated with the parameter  $b$ . These plots were made with 500 values for  $R$  and  $\Psi$ .

## 2.2. Object Creation

In order to calculate the flux, the coordinates of each subdivision of the accretion columns are needed. This was obtained by the *pymesh* platform in python. The mesh of the star and its accretion columns can be created by adding and subtracting three dimensional geometrical forms. We have used cylindrical and cone trunks. The top of each column is closed with a spherical cap, in order that a column tends to a polar cap as its height tends to zero. Additionally, *pymesh* provides the objects (stellar surface and columns) subdivisions, its baricenters, and its normal vectors, which are all needed to perform the calculations. Figure 1 shows how the accretion columns are visualized by the simulation.

## 2.3. Flux Calculation

Given the coordinates of an emitting subdivision of the column, its flux is calculated by ([12])

$$dF = I' \delta^4 (1 - u)^2 \cos \gamma' \frac{dS'}{D^2}, \quad (4)$$

where  $I'$  is the intensity in the corotating frame,  $\delta$  is the Doppler shift,  $u = r_s/r$ ,  $\gamma'$  is the angle between the direction of emission and the normal to the element, and  $dS'$  is the area of the element and  $D$  the distance to the source. The  $\delta^4(1 - u)^2$  term accounts for Doppler and gravitational redshift effects. For the present analysis, an isotropic blackbody emission from the columns is assumed since our purpose here is to see geometrical effects only. Additionally, the distance of the source to the observer is not a necessary feature since the flux is normalized through

$$F_{norm} = \frac{F}{(F_{max} + F_{min})/2}. \quad (5)$$

After the flux for each subdivision is calculated, the star is rotated around its rotational axis, starting the flux count from the beginning. This process is repeated until the flux for the whole rotation is obtained.

## 2.4. Data Selection and Reduction

The data employed to constrain the parameters of 1A 0535+262 were retrieved from its longest available observation from the NuSTAR mission [13] archival database. This observation (ObsID 90401370001) occurred on 26 December 2018, three months after the type-I outbursts, when the source was in a deep quiescent state with luminosities as low as  $\sim 7 \times 10^{34} \text{ erg s}^{-1}$  [14]. The observation lasted (total span time) approximately 33 h, with an effective on-source time (i.e., exposure time) of about 15 h ( $\sim 55 \text{ ks}$ ).

Data were reduced following the standard procedures of the NuSTAR Data Analysis Software (NUSTARDAS pipeline v2.0); calibration files from CALDB version 20210427 were used. The source and background to generate lightcurves were extracted, respectively, from a  $\sim 75 \text{ arcsec}$  region centred on the source position and from a source-free region—on the same detector—of  $\sim 95 \text{ arcsec}$ . A Barycenter correction with the FTOOL *barycorr* was applied.

## 2.5. Genetic Algorithm

Inspired by natural selection, the genetic algorithm (GA) is a programming technique in which the parameters, e.g., M and R, are treated as genes and a set of free parameters are treated as chromosomes. Following natural evolution, these chromosomes' phenotype, the pulse profile, must adapt to its surroundings, the data.

That said, the GA can be described by the following steps:

1. Initialization: the generation of a population of solutions (i.e., the chromosomes);
2. Phenotype evaluation: the calculation of each model solution's fitness;
3. The selection of the best solutions;
4. Reproduction: the genes of the best solutions are recombined;

5. Mutation: genes can be randomly selected and changed;
6. Population replacement.

The set composed of steps 2 to 6 is called a generation. In step 3, the best solutions are selected through the goodness-of-fit ( $\chi$ ) of a given solution, representing the square difference between the model and the observed data ,

$$\chi^2 = \sum_k [\bar{F}_k^{TOT} - \bar{F}_k^{OBS}]^2, \quad (6)$$

where  $\bar{F}_k^{TOT}$  is (4) summed over all observed points in an instant of rotation, normalized by Equation (5).  $\bar{F}_k^{OBS}$  is the normalized observed flux of our data , and  $k = 1 - N$ , where  $N$  is the number of points observed in the lightcurve, so the difference in flux is summed over the period of the pulse profile. The best fit will have its  $\chi^2$  closer to zero [7].

In the present work, the GA has the sole objective of finding an adequate prior probability distribution for the Markov Chain Monte Carlo (MCMC) method. Then, the MCMC algorithm is able to evolve the prior distribution according to Bayes' Theorem until a convergence criterion is reached. The MCMC method is discussed in the next section.

### 2.6. Markov Chain Monte Carlo

The Markov chain Monte Carlo (MCMC) method is a Bayesian sample method, i.e., it is based on the Bayes' theorem given by

$$P(A|B) = \frac{P(B|A)P(A)}{P(B)}, \quad (7)$$

where, in statistical language,  $P(A)$  is the prior probability,  $P(B|A)$  is the likelihood probability, and  $P(A|B)$  is the posterior probability. The  $P(B)$  is not important in the applied method.

In order to run the algorithm, a prior probability distribution must be provided. The prior is supposed to reflect our prior knowledge of each variable in the model. The genetic algorithm is responsible for producing the mean values for such distributions (see Section 2.5). Then, normal distributions are built around the mean values, which become the input distributions for the MCMC algorithm.

The likelihood  $P(B|A)$  is the conditional probability distribution that given the true parameter value being  $A$ , the output  $B$  is observed. For a sample set, where the most recent is  $\theta_k$ , the next sample is generated by the following:

1. Sampling: A parameter set  $\theta'$  is taken from a proposal, a probability distribution function.
2. Evaluation: The new set is evaluated to know whether it is more likely or not by the ratio  $f(\theta')/\theta_k$ .
3. Selection: If it is more likely,  $\theta'$  will be the new sample. Otherwise, the algorithm accepts it anyway within a predefined probability.

Where  $f(\theta)$  is the prior times the likelihood [15].

### 3. Results

Figure 5 shows the parameter space, i.e., the posterior probability, for  $M$  and  $R$  calculated as depicted in Sections 2.5 and 2.6. For this result, we considered two columns with independent positions, cone trunk shapes, and a column height fixed at 1 km. The fit for 1A 0535+262 suggests  $M = 1.53_{-0.40}^{+0.52} M_{\odot}$  and  $R = 12.11_{-0.87}^{+1.14}$  km at  $1\sigma$  (68%) confidence level (CL). Other parameters can be found in Table 1. Figure 6 shows a comparison between the observed data and the fitted theoretical model.

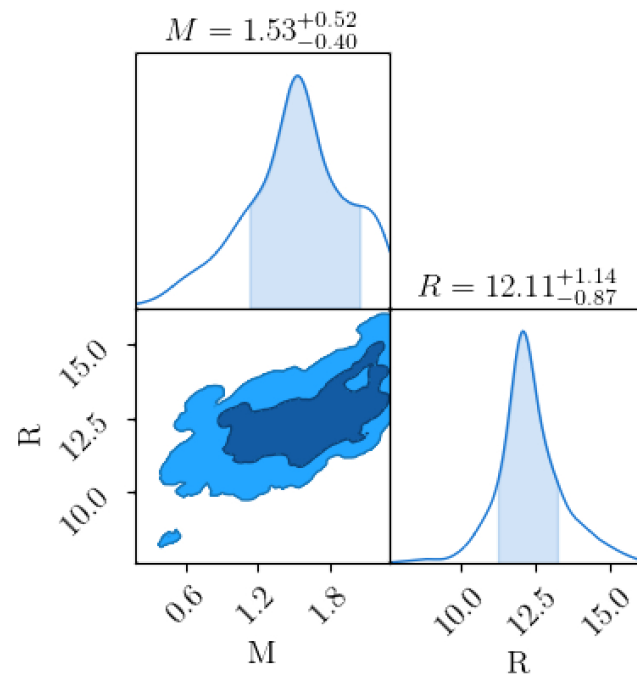


**Figure 5.** Parametric space at  $1\sigma$  CL and one-dimensional marginalized distribution of  $M$  and  $R$  for two hot spots on the surface of 1A 0535+262. For completeness,  $M$  and  $R$  are measured in units of  $M_{\odot}$ , and km, respectively. The dark (light) blue shows the parametric space at  $1\sigma$  ( $2\sigma$ ) CL.

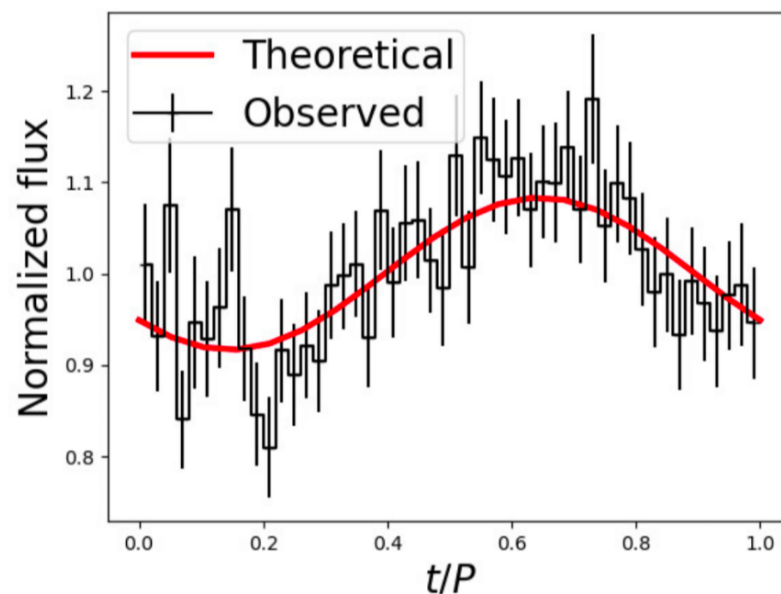


**Figure 6.** Phase diagram for the set of best parameters calculated in the posterior of the MCMC algorithm.

Figure 7 shows the phase diagrams for one column with height  $H = 1.0$  km and different values for the semi-aperture  $\theta_0$ , e.g.,  $5^\circ$ ,  $10^\circ$ ,  $20^\circ$ , and  $30^\circ$ . As expected, bigger apertures imply more pencil beam rays due to the increasing column area. Because of the rotation, sometimes, throughout the phase, the pencil beams are emitted in the observer direction (LOS). This increases the pulsed fraction with the widening of the difference between the higher flux and the lower one. Figure 8 shows the importance of the fan beams when  $H \sim 1.0$  km. This contribution for the flux is dependent on the form of the column, as one can see in the lower plots of Figure 8. The reason for this is that, as defined

here, both have the same base size, i.e., the spot size, and therefore the cone trunk has more emission surface than the cylindrical column.

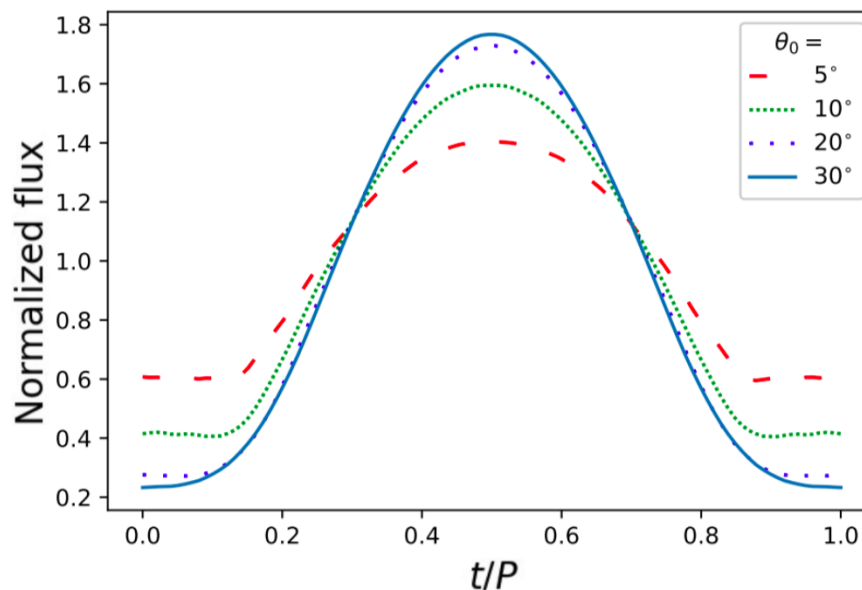


**Figure 7.** Phase diagrams for different values of angular semi-aperture  $\theta_0$ . The results are calculated for a column of height  $H = 1.0$  km. The parameters are  $M = 1.4 M_\odot$ ,  $R = 12.0$  km,  $i = 90^\circ$ ,  $P = 1$  s,  $\theta = 45^\circ$ , and  $\phi = 180^\circ$ ,  $T = 0.7$  KeV.

**Table 1.** Best solutions with the parameters of the two accretion columns.

Best Solutions	
$M(M_\odot)$	$1.53^{+0.52}_{-0.40}$
$R(\text{km})$	$12.11^{+1.14}_{-0.87}$
$i$	$4.93^{+0.96}_{-1.22}$
$\theta_1$	$50.4^{+2.3}_{-2.0}$
$\theta_{0\ 1}$	$72.3^{+2.1}_{-2.0}$
$T_1(\text{keV})$	$0.404^{+0.047}_{-0.066}$
$\theta_2$	$321.1^{+1.7}_{-1.7}$
$\theta_{0\ 2}$	$48.0^{+1.1}_{-1.2}$
$T_2(\text{keV})$	$59.31^{+0.99}_{-0.98}$
$\phi_2$	$0.955^{+0.035}_{-0.154}$

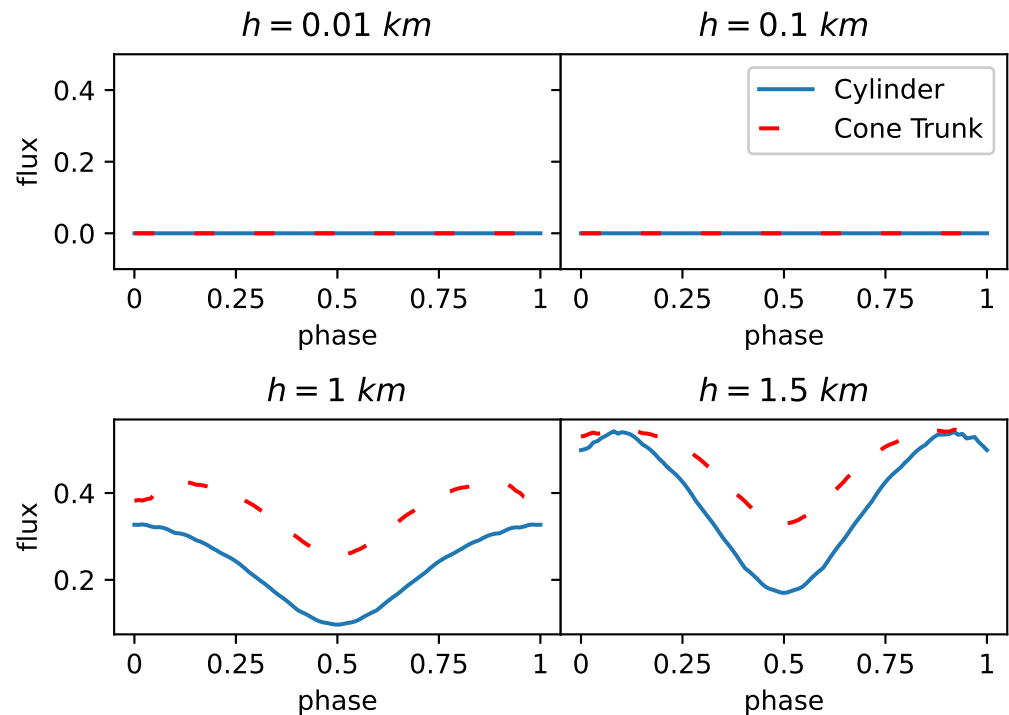


**Figure 8.** The fan beam phase diagrams for different column heights are shown. Blue continuous (red discontinuous) lines show results for cylindrical (cone trunks) columns. Parameters:  $M = 1.4M_{\odot}$ ,  $R = 12$  km,  $i = 90^{\circ}$ ,  $P = 1$  s,  $\theta_{10} = 15^{\circ}$ ,  $\theta_1 = 45^{\circ}$ ,  $\phi_1 = 180^{\circ}$ , and  $T_1 = 0.7$  keV.

#### 4. Summary

The simulation developed can create a pulse profile of a neutron star with accretion columns given a set of parameters ( $M$ ,  $R$ ,  $f$ ,  $i$ ,  $\theta_0$ ,  $\theta$ ,  $\phi$ ,  $H$ ,  $T$ ), where the last four are given for each column. Some features of the pulse profile for that emission were observed, such as the increase in the flux due to the fan beam, as well as the change due to the chosen geometry for the column. With the assistance of sample algorithms, a set of parameters for the neutron star and the columns were constrained for the source 1A 0535+262.

**Author Contributions:** Conceptualization, R.C.R.d.L.; methodology, R.C.R.d.L. and R.R.S.; software, R.R.S. and C.M.d.L.; data curation, P.E.S.; writing—original draft preparation, J.G.C. and R.R.S.; writing—review and editing, J.G.C. and R.R.S.; supervision, J.C.N.d.A. and J.G.C. All authors have read and agreed to the published version of the manuscript.

**Funding:** R.R.S. is grateful for the support of CAPES. R.C.R.d.L. acknowledges the support of Fundação de Amparo à Pesquisa e Inovação do Estado de Santa Catarina (FAPESC) under grant No. 2021TR912. J.G.C. is grateful for the support of CNPq (311758/2021-5), FAPESP (2021/01089-1), and NAPI “Fenômenos Extremos do Universo” of Fundação Araucária. P.E.S. acknowledges PCI/INPE/CNPq for financial support under grant #300320/2022-1.

**Institutional Review Board Statement:** Not applicable.

**Informed Consent Statement:** Not applicable.

**Data Availability Statement:** The data and the code underlying this article will be shared on reasonable request to the corresponding author.

**Acknowledgments:** We thank the referees for the thoughtful comments and suggestions that helped us to improve the presentation of our results.

**Conflicts of Interest:** The authors declare no conflict of interest.

## References

1. Mészáros, P. Radiation from accreting magnetized neutron stars. *Space Sci. Rev.* **1984**, *38*, 325. [[CrossRef](#)]
2. Patruno, A.; Watts, A.L. Accreting Millisecond X-ray Pulsars. In *Timing Neutron Stars: Pulsations, Oscillations and Explosions*; Belloni, T.M., Méndez, M., Zhang, C., Eds.; Springer: Berlin/Heidelberg, Germany, 2007; pp. 143–208.
3. Basko, M.; Sunyaev, R. The Limiting Luminosity of Accreting Neutron Stars with Magnetic Fields. *Mon. Not. R. Astron. Soc.* **1976**, *175*, 395–417. [[CrossRef](#)]
4. White, N.; Swank, J.; Holt, S. Accretion powered X-ray pulsars. *Astrophys. J.* **1983**, *270*, 711–734. [[CrossRef](#)]
5. Falkner, S. Light Bending around Neutron Stars. Master's Thesis, Fdr Karl Remeis Observatory Bamberg Astronomical Institute of the Friedrich-Alexander-University Erlangen-Nuremberg, Bamberg, Germany, 2012.
6. Beloborodov, A.M. Gravitational Bending of Light Near Compact Objects. *Astrophys. J. Lett.* **2002**, *566*, L85–L88. [[CrossRef](#)]
7. Lima, R.; Coelho, J.; Pereira, J.; Rodrigues, C.; Rueda, J. Evidence for a Multipolar Magnetic Field in SGR J1745-2900 from X-Ray Light-curve Analysis. *Astrophys. J.* **2020**, *889*, 165. [[CrossRef](#)]
8. Finger, M.; Wilson, R.; Harmon, B. Quasi-periodic Oscillations during a Giant Outburst of A0535+262. *Astrophys. J.* **1996**, *459*, 288–297. [[CrossRef](#)]
9. Rosenberg, F.D.; Eyles, C.J.; Skinner, G.K.; Willmore, A.P. Observations of a transient X-ray source with a period of 104 s. *Nature* **1975**, *256*, 628. [[CrossRef](#)]
10. Doroshenko, V.; Santangelo, A.; Doroshenko, R.; Caballero, I.; Tsygankov, S.; Rothschild, R. XMM-Newton observations of 1A 0535+262 in quiescence. *Astron. Astrophys.* **2014**, *561*, A96. [[CrossRef](#)]
11. Caballero, I.; Kraus, U.; Santangelo, A.; Sasaki, M.; Kretschmar, P. Analyzing X-ray pulsar profiles: Geometry and beam pattern of A 0535+26. *Astron. Astrophys.* **2011**, *526*, A131. [[CrossRef](#)]
12. Poutanen, J.; Beloborodov, A. Pulse profiles of millisecond pulsars and their Fourier amplitudes. *Mon. Not. R. Astron. Soc.* **2006**, *373*, 836–844. [[CrossRef](#)]
13. Harrison, F.; Craig, W.; Christensen, F.; Hailey, C.J.; Zhang, W.W.; Boggs, S.E.; Stern, D.; Cook, W.R.; Forster, K.; Giommi, P. The Nuclear Spectroscopic Telescope Array (NuSTAR) High-energy X-Ray Mission. *Astrophys. J.* **2013**, *770*, e103. [[CrossRef](#)]
14. Tsygankov, S.; Doroshenko, V.; Mushtukov, A.; Suleimanov, V.; Lutovinov, A.; Poutanen, J. Cyclotron emission, absorption, and the two faces of X-ray pulsar A 0535+262. *Mon. Not. R. Astron. Soc.* **2019**, *487*, L30–L34. [[CrossRef](#)]
15. Hilbe, J.; Souza, R.; Ishida, E. *Bayesian Models for Astrophysical Data*; Cambridge University Press: Cambridge, UK, 2017.

**Disclaimer/Publisher's Note:** The statements, opinions and data contained in all publications are solely those of the individual author(s) and contributor(s) and not of MDPI and/or the editor(s). MDPI and/or the editor(s) disclaim responsibility for any injury to people or property resulting from any ideas, methods, instructions or products referred to in the content.